NANO LETTERS
Cite This: Nano Lett. XXXX, XXX, XXX−XXX
Letter
pubs.acs.org/NanoLett

Orientational Epitaxy of van der Waals Molecular Heterostructures

Lu'an Guo,[†,‡] Yitao Wang,[‡] Dogan Kaya,[§] Richard E Palmer,[∥] Guangde Chen,[†] and Quanmin Guo*[,‡]

[†]Department of Applied Physics and Key Laboratory for Quantum Information and Quantum Optoelectronic Devices of Shaanxi Province, Xi'an Jiaotong University, Xi'an 710049, China

[‡]School of Physics and Astronomy, University of Birmingham, Edgbaston, Birmingham B15 2TT, U.K.

[§]Department of Electronics and Automation, Vocational School of Adana, Cukurova University, 01160 Cukurova, Adana, Turkey

[∥]College of Engineering, Swansea University, Bay Campus, Fabian Way, Swansea SA1 8EN, U.K.

ABSTRACT: The shape of individual building blocks is an important parameter in bottom-up self-assembly of nanostructured materials. A simple shape change from sphere to spheroid can significantly affect the assembly process due to the modification to the orientational degrees of freedom. When a layer of spheres is placed upon a layer of spheroids, the strain at the interface can be minimized by the spheroid taking a special orientation. C_{70} fullerenes represent the smallest spheroids, and their interaction with a sphere-like C_{60} is investigated. We find that the orientation of the C_{70} within a close-packed C_{70} layer can be steered by contacting a layer of C_{60}. This orientational steering phenomenon is potentially useful for epitaxial growth of multilayer van der Waals molecular heterostructures.

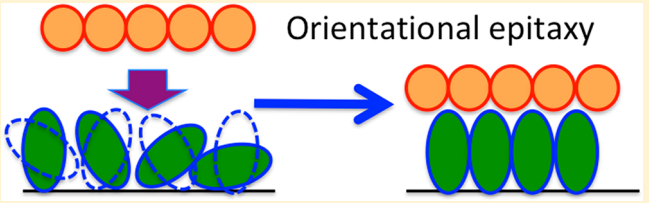

KEYWORDS: *van der Waals heterostructures, epitaxy, self-assembly, fullerene, graphene, interface, scanning tunnelling microscopy*

Epitaxial growth of thin films, a process extensively used in the semiconductor industry for fabricating electronic and optoelectronic devices,[1−4] has recently found applications in a number of emerging fields such as van der Waals heterostructures,[5−7] metal−organic frameworks (MOFs),[8] organic semiconductors,[9,10] and colloidal assembly.[11,12] In a typical heteroepitaxy process, a thin film of element A is grown on a crystalline substrate of element B. The thin film of A is normally under some stress, which arises from lattice mismatch between the two elements,[13] and consequently, there has been much interest in fabricating strained layers by deliberately introducing stress into the grown layers.[14−16] The structure of the interface depends not only on the lattice mismatch but also on the type of bonding involved.[17] For van der Waals epitaxy[17] where a layered material grows on top of another layered material such as the stacking of transition metal dichalcogenides (MoS_2, WSe_2, etc.), multilayer stacks of high quality 2D materials can be formed in the presence of very large lattice mismatch.[17] For such 2D materials, the formation of an epitaxial layer is mainly controlled by the strong atomic bonding within the layer, with the weak van der Waals interaction between the layers playing a much less significant role.

The term "van der Waals epitaxy" should not be restricted to the epitaxial growth of the conventional van der Waals heterostructures.[5−7] By introducing organic molecules, for example, hybrid organic/inorganic van der Waals heterostructures have been made.[18] The self-assembly of organic molecules on top of 2D materials opens up new avenues for fabricating hybrid functional materials.[18] Layered materials can also be produced by stacking organic molecules based completely on van der Waals interactions. One can take the layer-by-layer approach[19] to synthesize a molecular material consisting of alternating layers of two molecules (A and B). Molecules within both the A and B layers are bonded via van der Waals interaction. The bonding between the A and B layers is also van der Waals in nature. Without any specific interaction such as hydrogen bonding or ionic bonding, controlling the interfacial structure between two van der Waals molecular layers can be a real challenge. Here, we investigate the structure of the C_{60}/C_{70} interface. By depositing C_{60} and C_{70} sequentially onto highly oriented pyrolytic graphite (HOPG) at room temperature, a van der Waals bilayer is produced. There are two interesting aspects of this bilayer system. (i) Both molecules are significantly larger than typical atoms, but much smaller than colloidal particles. The system serves as a good example to understand size scalability in nucleation and growth.[20] (ii) The different shapes of the two molecules offer a good example to study the packing of objects with different geometric forms.[21,22]

C_{60} is a useful component in organic solar cells[23,24] and in molecular p−n heterojuctions.[10] When combined with gold atoms, C_{60} molecules are able to assemble into hybrid magic number clusters[25,26] or nanorings.[27] The assembly of C_{60} on various atomically flat solid substrates has been extensively studied.[28−35] It has been found that C_{60} molecules have strong

Received: June 2, 2018
Revised: July 12, 2018
Published: July 12, 2018

DOI: 10.1021/acs.nanolett.8b02238
Nano Lett. XXXX, XXX, XXX−XXX

tendency to form close-packed layers and do so on many solid surfaces where the molecule−substrate interaction is relatively weak. Investigations of C_{60} and C_{70} mixture have found several bulk phases of the $(C_{60})_{1-x}(C_{70})_x$ alloy and a miscibility gap.[36,37] The mixing of these two molecules has also been studied using high-resolution scanning tunnelling microscopy (STM).[38,39] The direct interaction between a close-packed C_{60} layer with a C_{70} layer has not been studied so far. Due to the different lattice parameters, a C_{60}−C_{70} bilayer is expected to be strained with tensile stress in the C_{60} layer and compressive stress in the C_{70} layer. How the bilayer accommodates the strain is an interesting problem. In addition to the usual ways of strain relief such as the introduction of dislocations, the C_{70} molecule has a property that atoms do not have. The C_{70} molecule can take at least two different orientations: (i) with the long axis perpendicular to the interface or (ii) with the long axis parallel to the interface. This extra degrees of freedom in molecular orientation provides additional channels for strain relief at the interface. Here, we report findings on the orientational switching of the C_{70} molecule and the detailed structure of the C_{60}−C_{70} interface.

Figure 1a shows an STM image acquired from a region of the HOPG sample covered by a monolayer of molecules. The sample was prepared by sequentially deposition of 1.2 monolayers (ML) of C_{70} and 0.2 ML of C_{60} at RT. It was then annealed at 425 K for 30 min to initiate some mixing of the two molecules. Parts of the substrate are covered by multiplayers. Here, we concentrate on this particular region where a C_{60}-rich layer (single layer) sits next to a C_{70}-rich layer (single layer), with both the C_{60}-rich and the C_{70}-rich layers sitting directly above the HOPG substrate. The direction of close-packed molecules is the same for both C_{60} and C_{70} in this image. This may arise from some specific interactions at the C_{60} and C_{70} boundary. In Figure 1a, the distance defined by the two parallel yellow lines accommodates 14 rows of C_{70} and 15 rows of C_{60}. Thus, the ratio of the nearest neighbor C_{70}−C_{70} distance to that of the C_{60}−C_{60} distance is 1.07. Taking the nearest neighbor C_{60}−C_{60} distance as 1.0 nm,[40] the nearest neighbor C_{70}−C_{70} distance is found to be 1.07 nm. These values are in good agreement with those found in the bulk fullerites using X-ray diffraction (XRD),[41] indicating that the structure of the monolayer fullerenes on HOPG is very close to the bulk projection of the (111) plane of the corresponding fullerite.

The crystalline C_{70} has an fcc structure at temperatures above 340 K. In this fcc phase, the C_{70} molecule rotates freely with no orientational order. The nearest neighbor distance in the fcc phase is 1.06 nm.[41] Below 340 K, a phase transition occurs such that the long axis of the C_{70} molecule becomes frozen in the direction perpendicular to one of the close-packed layers. As a consequence, the in-plane nearest neighbor C_{70}−C_{70} distance is reduced from 1.06 to 1.01 nm. The 1.07 nm nearest neighbor C_{70}−C_{70} distance measured by our STM is a good indication that the C_{70} molecules within the first C_{70} layer on HOPG is rotationally disordered even at RT.

Figure 1b displays the height profile along the blue line in Figure 1a. In this profile, the tallest feature (C_{70}-U, U for upright), 0.11 nm taller than C_{60}, corresponds to an isolated C_{70} molecule trapped inside the C_{60}-rich domain. In Figure 1a, there are approximately 1% of C_{60} molecules within the C_{60}-rich domain substituted by trapped C_{70} molecules. The trapped C_{70} occupies the space vacated by a C_{60} molecule. Due to steric hindrance, the trapped C_{70} can only take an orientation with its long axis perpendicular to the substrate. By having the long axis perpendicular to the substrate, a trapped C_{70} molecule inside the C_{60} domain has the same footprint as a C_{60}. This is a favorable configuration because of the nearly zero strain introduced into the C_{60} lattice by substituting a C_{60} with a C_{70} in such a manner. The 0.11 nm height difference between the trapped C_{70} and the C_{60} molecules is consistent

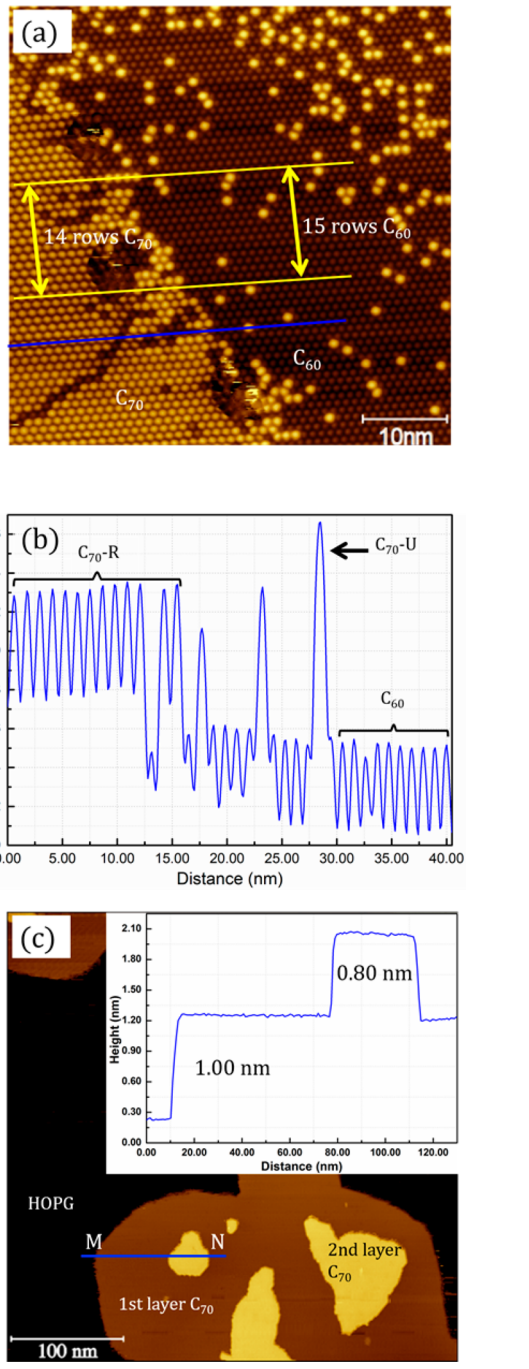

Figure 1. (a) STM image acquired at RT from HOPG covered by a single layer of C_{60}/C_{70}. There is a C_{70}-rich domain to the left and a C_{60}-rich domain to the right of the image. The bright features inside the C_{60} domain are trapped C_{70} molecules. C_{60} molecules inside the C_{70}-rich domain seem to have aggregated into zigzag rows. (b) Height profile along the blue line in (a). (c) Layers of C_{70} on HOPG following RT deposition. The 2nd layer forms before the first layer is completed. Inset is the height profile measured along line M−N.

DOI: 10.1021/acs.nanolett.8b02238
Nano Lett. XXXX, XXX, XXX−XXX

with this conclusion. Height measured by STM has electronic contributions as well as geometric contributions, and it is not always straightforward to separate the two contributions. The height profile shown in Figure 1b is independent of the bias voltage, suggesting mainly a geometric contribution. Moreover, charge transfer between HOPG and the fullerenes is expected to be weak, making any electronic contribution to the height measurement insignificant.

The C_{70} molecules inside the C_{70}-rich domain (C_{70}-R, R for rotation) appear lower than the trapped C_{70} molecules by 0.04 nm. This is because the molecules inside the closed-packed C_{70} domain do not have a fixed orientation. They are under constant rotation. When a free-rotating C_{70} is being imaged by the STM, it can be regarded as spending part of its time with the long axis perpendicular to the substrate and the rest of the time with the long axis parallel to the substrate. With the molecular rotation taking place at a much faster rate than the response time of the STM tip, an effective tunnel current is registered. If the tip height is fixed, the effective tunnel current would be lower when the tip is above a rotating C_{70} molecule than when it is above an upright C_{70} molecule.

Figure 1c shows an STM image acquired from the HOPG sample after 1.2 ML of C_{70} is deposited at RT. The second molecular layer is formed before the first layer is completed. The inset in Figure 1c shows a height profile measured along the blue line M−N. Based on this height profile, the first layer measured from the HOPG surface is 1.00 nm tall. The second layer is 0.80 nm above the first layer. The ratio of 1.00/0.80 is consistent with two layers of close-packed hard spheres with the second layer spheres sitting in the 3-fold hollow site of the first layer. For C_{60} on HOPG, the first layer is 0.80 nm above the HOPG substrate, and the second C_{60} layer is 0.70 nm above the first layer.

Figure 2a shows an STM image from the sample after adding 0.2 ML of C_{70} molecules onto the HOPG with a pre-existing 1.2 ML of C_{60}. The C_{70} molecules are found to attach to the edges of the preformed C_{60} islands in both the first and the second layers. The second layer C_{60} has the same lattice parameter as the first layer. However, the second layer C_{70} has a smaller lattice parameter than C_{70} in the first layer. Figure 2c shows a boundary between the second layer C_{60} and the second layer C_{70}. This boundary is noticeable mainly because of the height difference between the two molecules. The C_{70} domain merges seamlessly with the neighboring C_{60} domain without the presence of any dislocations at the boundary. Therefore, the second layer C_{70} is lattice-matched with the underlying C_{60} layer, and this can only be achieved if the C_{70} molecules take the upright configuration with their long axis perpendicular to the surface. The C_{60}−C_{70} boundary in the second layer is sharp with no signs of intermixing. This suggests a rigid island boundary for the second layer C_{60}. The C_{70} rim in the first layer has C_{60} molecules incorporated. This is because the island edges of the first layer C_{60} are rather "fluidic" at RT, and there exists a two-dimensional vapor-like C_{60} phase in the vicinity of the C_{60} islands. Postdeposited C_{70} are thus able to mix with the C_{60} "vapor" before condensing into the rim. From the data shown in Figure 2, we can conclude that the first layer C_{60} has a steering effect on the orientation of the C_{70} molecules sitting directly above. The C_{70} molecules stand upright with their long axis perpendicular to the substrate. As a consequence, the second layer C_{70} has an excellent lattice match with the C_{60} layer below. Figure 3a shows a schematic diagram illustrating how the second layer C_{70} molecules form lattice-matched structure with C_{60}. Figure 3b indicates a possible structure if C_{60} molecules are postdeposited onto an existing C_{70} layer if all C_{70} molecules have the same upright orientation.

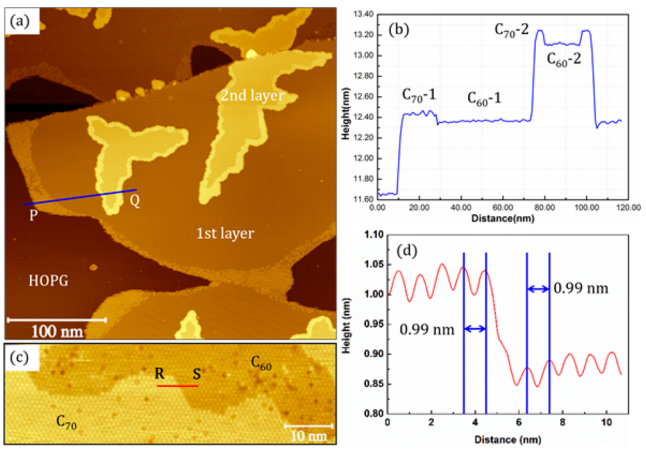

Figure 2. (a) STM image of the sample after 0.2 ML of C_{70} are added to a pre-existing 1.2 ML of C_{60} at RT. The postdeposited C_{70} form rims around the preformed C_{60} islands. (b) Height profile along line P−Q in (a). Characteristic heights corresponding to the first layer C_{60} (C_{60}-1), first layer C_{70} (C_{70}-1), second layer C_{60} (C_{60}-2), and second layer C_{70} (C_{70}-2), respectively, are clearly identified. (c) STM image showing a boundary between C_{60} and C_{70} in the second layer. (d) Height profile along line R−S in (c).

Figure 3c is an STM image from the sample after 0.2 ML of C_{60} molecules are deposited onto a preformed 1.2 ML of C_{70}. The image is displayed with enhanced contrast to compare the second layers of C_{60} and C_{70}. The first layer C_{70} can be seen in the original image but not visible in this processed image. The boundary between C_{60} and C_{70} in the second layer can be identified by a narrow region of uneven height contrast, highlighted with dashed lines. The C_{60} molecules appear to have the same height as C_{70} molecules in the second layer. However, the C_{60} domain has a smaller lattice parameter. As can be seen in Figure 3c, within the distance covered by the length of the double-headed arrows, there are 16 rows of C_{60} within the C_{60} domain. The same distance is occupied by 15 rows of C_{70} molecules inside the C_{70} domain. This 16/15 ratio is roughly the same, subject to experimental error, as that found from Figure 1 for the first layer molecules. We have repeated such measurement in different areas of the sample and found a consistent value for this ratio. The schematic diagram in Figure 3d is used to explain the characteristics in Figure 3c. We already know that C_{70} molecules in the first layer have complete freedom of rotation. When C_{60} molecules are added on top of the C_{70} first layer, the C_{60} molecules can choose either to sit in the hollow site and form a strained layer under tensile stress, or to form a strain-free layer by forcing the first layer C_{70} to stand upright. Our data indicates that the second layer C_{60} has formed a nearly strain-free layer. We cannot claim that there is absolutely zero strain although any residual strain is expected to be insignificantly low. This postformed second layer C_{60} thus forces the underlying C_{70} to stand upright leading to a lattice-matched interface. The interaction between the second layer C_{70} and the first layer C_{70}, however, does not help to improve the orientational ordering. C_{70} molecules in both the first and second layers are in their free rotating state. The height of two layers of free-

DOI: 10.1021/acs.nanolett.8b02238
Nano Lett. XXXX, XXX, XXX−XXX

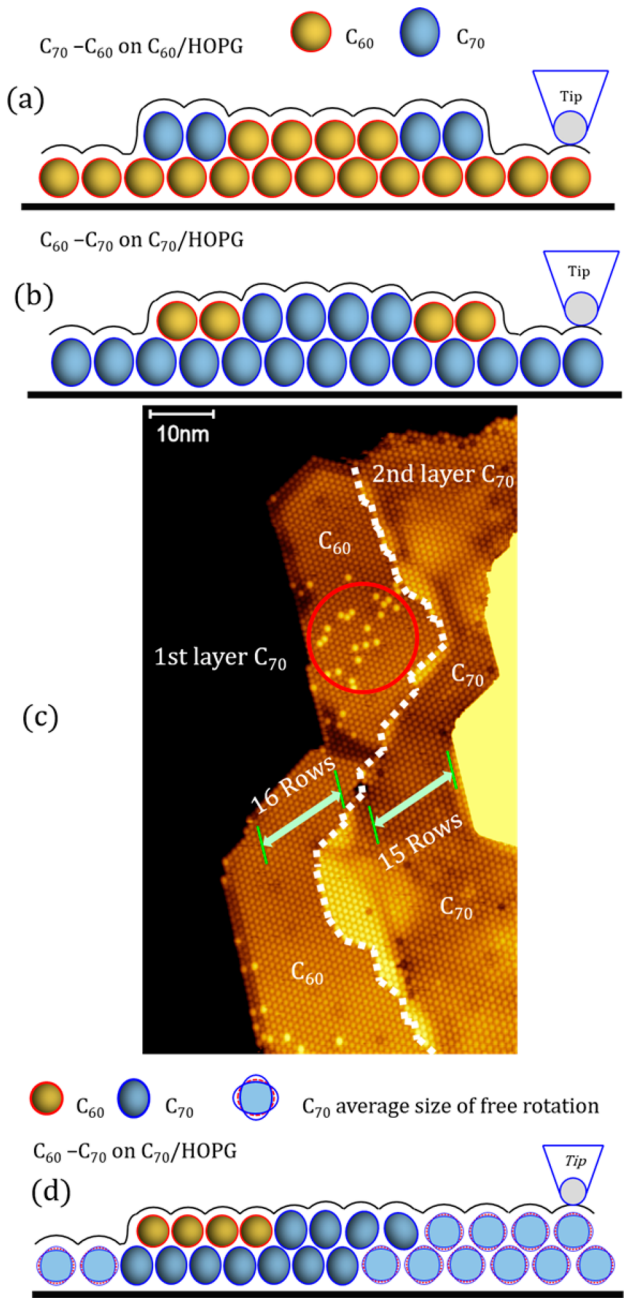

Figure 3. (a) Schematic of the tall C_{70} rim formed around a C_{60} island in the second layer. (b) Possible structure of a short C_{60} rim formed around a second layer C_{70} island. (c) STM image showing two interconnecting C_{60} and C_{70} domains in the second layer. They both sit on a first layer C_{70}. Following the deposition of C_{60}, the sample was annealed to 425 K for 30 min. Dashed lines highlight the boundary between C_{60} and C_{70}. Some scattered C_{70} molecules possibly due to the effect of annealing at 425 K, highlighted by the red circle, are observed within the C_{60} domain. The C_{60} and C_{70} domains can be distinguished by their different lattice parameters, rather than their heights. (d) Proposed structural model for the interface between first layer C_{70} and the second layer C_{60}.

rotating C_{70} molecules is comparable to the height of a C_{60} layer standing above a C_{70} layer with the upright orientation. From the data shown in Figure 1, we find that the upright C_{70} molecules are taller than the rotating molecules by 0.04 nm. This makes the height of C_{60} + C_{70}-U 1.70 nm, and the height of two layers of C_{70}-R 1.72 nm. Along the C_{60}–C_{70} boundary, there are a small number of tall C_{70} molecules. Thus, along the boundary, some C_{70} molecules are approximately standing upright. As can be seen in Figure 3c, this transition region at the boundary does not appear to have any long-range order. C_{60} induced orientational ordering of C_{70} relies on a rather weak C_{70}–HOPG interaction. If HOPG is substituted with another substrate that forms a strong directional bond with C_{70}, the C_{70} molecule may not be able to alter its orientation.

A challenging task is to grow a van der Waals solid consisting of alternating C_{60} and C_{70} layers. This is highly desirable in view of making new materials with tunable properties. One of the difficulties for growing such well-controlled multilayer structures is to achieve layer-by-layer growth. Under the standard growing conditions, we always observe the appearance of the second layer islands before the first layer is completed. The second layer islands subsequently affect the formation of the whole second layer. By experimenting with the deposition flux and the sample temperature, there is some possibility of finding an optimized condition for pure layer-by-layer epitaxy.

In summary, the ellipsoidal shape of C_{70} can make significant contributions to the structure of the C_{60}–C_{70} interface. By choosing an orientation that lattice matches the close-packed C_{60} layer, a strain-free heterostructure can be obtained. This scheme allows the fabrication of lattice-matched C_{60}–C_{70} multilayers. Giving up some degrees of rotational freedom leads to a reduced entropy of the C_{70} layer. This reduction in entropy is overcompensated by the reduced interfacial energy. The phenomenon of orientational epitaxy discovered for the C_{60}–C_{70} system is expected to be operative for other systems involving particles with nonspherical symmetry and scalable up to nanoparticles or colloidal systems.[21,42,43]

Methods. Highly oriented pyrolytic graphite (purchased from Goodfellow, 99.99% purity) was used as the substrate. The HOPG sample was cleaned by annealing in ultrahigh vacuum (UHV) at 475 K for 30 min to remove surface contamination just before deposition. C_{60} and C_{70} molecules (purchased from MER, 99.5% purity) were sublimed onto the HOPG substrate using home-built effusion cells. The effusion cells were degassed at 500 K for 5 min before sublimation. Then the C_{60} and C_{70} molecules were deposited on the surface with a rate of 0.12 and 0.10 ML/min, respectively. During deposition, the background pressure in the UHV system did not exceed 10^{-9} mbar. STM imaging was performed with an Omicron UHV variable temperature STM using electrochemically etched tungsten tips. Images were collected in constant current mode with tunnelling current set at 0.1 nA and bias voltage in the range between +2.00 and +2.58 V.

AUTHOR INFORMATION

Corresponding Author

*E-mail: q.guo@bham.ac.uk. Tel: +44 1214144657.

ORCID

Lu'an Guo: 0000-0003-0520-3600

Richard E Palmer: 0000-0001-8728-8083

Quanmin Guo: 0000-0002-3417-8726

Notes

The authors declare no competing financial interest.

ACKNOWLEDGMENTS

We thank the Chinese Scholarship Council for providing a studentship to L.G.

DOI: 10.1021/acs.nanolett.8b02238
Nano Lett. XXXX, XXX, XXX–XXX

REFERENCES

(1) Faist, J.; Capasso, F.; Sivco, D. L.; Sirtori, C.; Hutchinson, A. L.; Cho, A. Y. *Science* **1994**, *264*, 553−556.
(2) Yan, R. S.; et al. *Nature* **2018**, *555*, 183−189.
(3) Venables, J.; Spiller, G.; Hanbucken, M. *Rep. Prog. Phys.* **1984**, *47*, 399−459.
(4) Zhang, Z.; Lagally, M. G. *Science* **1997**, *276*, 377−383.
(5) Fu, D. Y.; et al. *J. Am. Chem. Soc.* **2017**, *139*, 9392−9400.
(6) Lin, M.; et al. *J. Am. Chem. Soc.* **2013**, *135*, 13274−13277.
(7) Jariwala, D.; Marks, T. J.; Hersam, M. C. *Nat. Mater.* **2017**, *16*, 170.
(8) Falcaro, P.; et al. *Nat. Mater.* **2017**, *16*, 342.
(9) Eremtchenko, M.; Schaefer, J. A.; Tautz, F. S. *Nature* **2003**, *425*, 602−605.
(10) Nakayama, Y.; et al. *ACS Appl. Mater. Interfaces* **2016**, *8*, 13499−13505.
(11) Ganapathy, R.; Buckley, M. R.; Gerbode, S. J.; Cohen, I. *Science* **2010**, *327*, 445−448.
(12) Gabrys, P. A.; et al. *Nano Lett.* **2018**, *18*, 579−585.
(13) Palmstrom, C. J. *Annu. Rev. Mater. Sci.* **1995**, *25*, 389−415.
(14) Xie, S.; Tu, L.; Han, Y.; Huang, L.; Kang, K.; Lao, K. U.; Poddar, R.; Park, C.; Muller, D. A.; DiStasio, R. A.; Park, J. *Science* **2018**, *359*, 1131−1136.
(15) Schlom, D. G.; et al. *MRS Bull.* **2014**, *39*, 118−130.
(16) Wang, R.; Lange, F. R. L.; Cecchi, S.; Hanke, M.; Wuttig, M.; Calarco, R. *Adv. Funct. Mater.* **2018**, *28*, 1705901.
(17) Koma, A. *Thin Solid Films* **1992**, *216*, 72−76.
(18) Gobbi, M.; Orgiu, E.; Samori, P. *Adv. Mater.* **2018**, *30*, 1706103.
(19) Richardson, J. J.; Cui, J.; Bjornmalm, M.; Braunger, J. A.; Ejima, H.; Caruso, F. *Chem. Rev.* **2016**, *116*, 14828−14867.
(20) Kleppmann, N.; Schreiber, F.; Klapp, S. H. L. *Phys. Rev. E: Stat. Phys., Plasmas, Fluids, Relat. Interdiscip. Top.* **2017**, *95*, 020801.
(21) Damasceno, P.; Engel, M.; Glotzer, S. *Science* **2012**, *337*, 453−457.
(22) Meijer, J.-M.; Pal, A.; Ouhajji, S.; Lekkerkerker, H. N. W.; Philipse, A. P.; Petukhov, A. V. *Nat. Commun.* **2017**, *8*, 14352.
(23) Campoy-Quiles, M.; et al. *Nat. Mater.* **2008**, *7*, 158−164.
(24) Schmidt-Hansberg, B.; et al. *ACS Nano* **2011**, *5*, 8579−8590.
(25) Xie, Y.-C.; Tang, L.; Guo, Q. *Phys. Rev. Lett.* **2013**, *111*, 186101.
(26) Kaya, D.; Bao, D.-L.; Palmer, R. E.; Du, S.-X.; Guo, Q. *Nano Lett.* **2017**, *17*, 6171−6176.
(27) Xie, Y.-C.; Rokni Fard, M.; Kaya, D.; Bao, D.-L.; Palmer, R. E.; Du, S.-X.; Guo, Q. *J. Phys. Chem. C* **2016**, *120*, 10975−10981.
(28) Bommel, S.; Kleppmann, N.; Weber, C.; Spranger, H.; Schafer, P.; Novak, J.; Roth, S. V.; Schreiber, F.; Klapp, S. H. L.; Kowarik. *Nat. Commun.* **2014**, 5388.
(29) Freund, S.; Hinaut, A.; Pawlak, R.; Liu, S.-X.; Decurtins, S.; Meyer, E.; Glatzel, T. *ACS Nano* **2016**, *10*, 5782−5788.
(30) Korner, M.; Loske, F.; Einax, M.; Kuhnle, A.; Reichling, M.; Maass, P. *Phys. Rev. Lett.* **2011**, *107*, 016101.
(31) Zhang, X.; Tang, L.; Guo, Q. *J. Phys. Chem. C* **2010**, *114*, 6433.
(32) Li, H. I.; Pussi, K.; Hanna, K. J.; Wang, L. L.; Johnson, D. D.; Cheng, H. P.; Shin, H.; Curtarolo, S.; Moritz, W.; Smerdon, J.; McGrath, R.; Diehl, R. D. *Phys. Rev. Lett.* **2009**, *103*, 056101.
(33) Gardener, J. A.; Briggs, G. A. D.; Castell, M. R. *Phys. Rev. B: Condens. Matter Mater. Phys.* **2009**, *80*, 235434.
(34) Altman, E. I.; Colton, R. J. *Surf. Sci.* **1993**, *295*, 13.
(35) Tzeng, C. T.; Lo, W. S.; Yuh, J. Y.; Chu, R. Y.; Tsuei, K. D. *Phys. Rev. B: Condens. Matter Mater. Phys.* **2000**, *61*, 2263.
(36) Havlik, D.; Schranz, W. *Phase Transitions* **1999**, *67*, 779−788.
(37) Sai Baba, M.; Narasimhan, T. S. L.; Balasubramanian, R.; Sivaraman, N.; Mathews, C. K. *J. Phys. Chem.* **1994**, *98*, 1333−1340.
(38) Rossel, F.; Pivetta, M.; Patthey, F.; Cavar, E.; Seitsonen, A. P.; Schneider, W.-D. *Phys. Rev. B: Condens. Matter Mater. Phys.* **2011**, *84*, 075426.
(39) Olyanich, D. A.; Mararov, V. V.; Utas, T. V.; Zotov, A. V.; Saranin, A. A. *Surf. Sci.* **2016**, *653*, 138−142.
(40) Dresselhaus, M. S.; Dresselhaus, G.; Eklund, P. C. *Science of Fullerenes and Carbon Nanotubes*; Academic Press: New York, 1996.
(41) Vaughan, G. B. M.; Heiney, P. A.; Cox, D. E.; Fischer, J. E.; McGhie, A. R.; Smith, A.; Strongin, R. M.; Cichy, M. A.; Smith, A. B., III *Chem. Phys.* **1993**, *178*, 599−613.
(42) Donev, A.; Stillinger, F.; Chaikin, P. M.; Torquato, S. *Phys. Rev. Lett.* **2004**, *92*, 255506.
(43) Kang, C. J.; Honciuc, A. *ACS Nano* **2018**, *12*, 3741−3750.

DOI: 10.1021/acs.nanolett.8b02238
Nano Lett. XXXX, XXX, XXX−XXX